Latin American Journal of Solids and Structures
www.lajss.org

Finite Element Analysis of Reinforced Concrete Beam-Column Connections with Governing Joint Shear Failure Mode

Abstract

Reinforced concrete (RC) beam-column connections especially those without transverse reinforcement in joint region can exhibit brittle behavior when intensive damage is concentrated in the joint region during an earthquake event. Brittle behavior in the joint region can compromise the ductile design philosophy and the expected overall performance of structure when subjected to seismic loading. Considering the importance of joint shear failure influences on strength, ductility and stability of RC moment resisting frames, a finite element modeling which focuses on joint shear behavior is presented in this article. Nonlinear finite element analysis (FEA) of RC beam-column connections is performed in order to investigate the joint shear failure mode in terms of joint shear capacity, deformations and cracking pattern. A 3D finite element model capable of appropriately modeling the concrete stress-strain behavior, tensile cracking and compressive damage of concrete and indirect modeling of steel-concrete bond is used. In order to define nonlinear behavior of concrete material, the concrete damage plasticity is applied to the numerical model as a distributed plasticity over the whole geometry. Finite element model is then verified against experimental results of two non-ductile beam-column connections (one exterior and one interior) which are vulnerable to joint shear failure. The comparison between experimental and numerical results indicates that the FE model is able to simulate the performance of the beam-column connections and is able to capture the joint shear failure in RC beam-column connections.

Keywords

Finite element analysis, Concrete damage plasticity, RC beam-column connection, Joint shear failure, Numerical model.

M.A. Najafgholipour [a]
S.M. Dehghan [b]
Amin Dooshabi [c]
Arsalan Niroomandi [d]

[a] Faculty of Civil and Environmental Engineering, Shiraz University of Technology, Shiraz, Iran, najafgholipour@sutech.ac.ir
[b] Faculty of Civil and Environmental Engineering, Shiraz University of Technology, Shiraz, Iran, smdehghan@sutech.ac.ir
[c] Graduate student of Civil and Environmental Engineering, Shiraz University of Technology, Shiraz, Iran
[d] Department of Civil and Natural Resources, University of Canterbury, Christchurch, New Zealand

http://dx.doi.org/10.1590/1679-78253682

Received 15.01.2017
In revised form 15.03.2017
Accepted 05.05.2017
Available online 26.05.2017

1 INTRODUCTION

Beam-column connection in Reinforced Concrete (RC) frame is one of the most critical parts of the structure which has important role in seismic performance of these buildings. When a beam-column connection of a moment resisting frame is subjected to lateral forces, beam-column joint is prone to joint shear failure due to high shear stress which appears in the joint panel as a result of opposite sign moments on both sides of the joint core. This type of failure is not favorable because it has undesirable effects on seismic performance of RC buildings, especially moment resisting frames. The joint shear failure is a brittle type of failure which can adversely affect ductility of the RC frames. Also, early occurrence of this failure causes the beams not to reach their ultimate flexural capacity. Finally, the exposure of severe damage in the joint region may lead to total collapse of the building when the structure is in the seismically active regions and designed according to non-seismic design guidelines before the application of modern seismic design codes (ACI 318-14, ACI 352R-02, ASCE 41-13 and NZS3101). Therefore, this type of failure has undesirable effects on global seismic performance of RC structures, especially moment resisting frames.

Considerable amount of experimental and analytical studies have been carried out to investigate the seismic performance of RC beam-column joints subjected to lateral earthquake loading (Elsouri and Harajli (2013), Lee et al. (2009), Masi et al. (2013) and Sasmal et al. (2013)) or development of retrofitting techniques for vulnerable existing RC beam column joints (Eslami and Ronagh (2014), Esmaeeli et al. (2014), Vecchio et al. (2016), Shwan and Abdul Razak (2016), Esmaeeli et al. (2015) and Campione et al (2015)). Some of these researches were concentrated on shear resistance and behavior of RC beam-column joints. As one of the first studies in this field Hanson and Connor (1967) suggested a quantitative definition of joint shear. Based on their definition, joint shear was determined from a free-body diagram, at mid-height of the joint panel. Pauley et al (1978) introduced qualitative analytical shear resistance mechanisms of RC beam-column joints including a concrete strut and a truss. The first mechanism is a diagonal compression concrete strut that transfers the compression forces from the beam and column actions without the contribution of shear reinforcement. The second mechanism is a stress mechanism that transfers bond forces from the longitudinal bars utilizing horizontal and vertical joint shear reinforcement and concrete struts, therefore the shear resistance in the joint region corresponding to concrete truss mechanism is attributed to the bond capacity between reinforcement and concrete. These basic studies were followed by experimental researches on RC joints aimed at evaluation of their shear behavior (De Risi et al. (2016), Kotsovou and Mouzakis (2012) and Hakuto et al. (2000)). The tests were done on different joint types such as exterior, interior, knee and T joints in different scales. In these experimental studies the effects of different parameters such as geometrical properties of the joint panel, concrete compressive strength, transverse joint reinforcement, beam longitudinal reinforcement, existence of RC slab, column axial load and etc. were investigated on the joint shear strength and load-displacement curves of the RC joints. Clyde et al (2000) and Pantelides et al (2002) carried out seismic tests on some half-scale exterior beam-column joint specimens in order to determine performance levels according to FEMA273 guidelines. Park and Mosalam (2012) tested four full-scale exterior beam-column joints with orthogonal transverse beams and floor slabs under variable column axial loads. They investigated the behavior of unreinforced exterior joints subjected to cyclic loading. Their investigation was focused on the effect of some crucial parameters, such as joint as-

pect ratio and beam longitudinal reinforcement ratio on the shear strength and deformability of exterior connection joints comparing their test results with the ASCE 41 seismic design recommendations.

A series of researchers have collected the test results in literature and have developed empirical and analytical relations to predict the RC joint shear capacity (Pauletta et al. (2015), Muhsen and Umemura (2011), Park and Mosalam (2012), Lima et al. (2012), Wong and Kuang (2014), Wang et al. (2012), Jeon et al. (2014) and Kassem (2016)). For example Kim and Lafave (2007) collected experimental results of semi-static cyclic tests carried out by different researchers on various types of RC beam-column connections (exterior, interior and corner joints). All specimens had a minimum amount of joint confinement and the main objective of the study was to investigate the most influential parameters affecting the joint shear load-displacement behavior. The parameters investigated were material property, joint panel geometry, confining reinforcement, reinforcement bond condition and the column axial force. A design approach for RC beam-column joint was presented by Kotsovou and Mouzakis (2012). The basic assumption of their model was that the load transferred from the linear elements to the joint is mainly resisted by a diagonal strut mechanism. In a state of the art article, Lima et al (2012) reviewed some of the analytical and empirical models introduced in the last two decades for predicting shear strength of RC beam-column joints. Some simplified models are also developed for simulation of the joint shear behavior in nonlinear static and dynamic analysis of RC frames (Sharma et al. (2011), Favvata et al. (2008) and Shayanfar et al. (2016)). For instance, model developed by Shayanfar et al (2016) is one of the recent models for this purpose. They have introduced a frame model to simulate the RC joints in nonlinear analysis of RC frames.

A series of numerical studies have been done on RC joints using FEM analysis. For example Niroomandi et al (2014) performed numerical investigation of affecting parameters on the shear failure of non-ductile exterior joints. According to their numerical results, two crucial parameters influencing the joint shear behavior were joint aspect ratio and beam longitudinal reinforcement ratio.

Although a majority of numerical studies have been carried out on RC beam-column connections (Parvin and Granata (2000), Mostofinejad and Talaeitaba (2006), Niroomandi et al (2010), Mahini and Ronagh (2011), Masi et al. (2013) and Haach et al. (2008)) by FEM softwares such as ANSYS, ABAQUS and DIANA, these studies have concentrated on simulating flexural behavior of beams and columns adjacent to the joint region and are not focused on joint shear behavior of RC connections, while in many cases the shear strength and behavior of joints control the overall response of RC beam-column connections subjected to seismic actions. It should be noted that capturing shear dominant failure mode in discontinuity region of connection is a very complicated numerical simulation problem.

The suggested modeling technique in this paper has been conducted by means of the commercial FEA program ABAQUS and calibrated by modeling and analyzing experimentally tested exterior and interior beam-column connections in which the governing failure mode during simulated seismic actions on the specimens was the joint shear failure type. The comparison between numerical and experimental results, indicates the ability of the proposed method in simulating the governing joint shear behavior even at post peak phase.

2 FINITE ELEMENT MODELING

Nonlinear finite element analysis of RC beam-column connections with joint shear failure as the governing failure mode is performed using ABAQUS/Standard. Geometrical and material nonlinearities are considered in order to properly simulate the behavior of connections and the joint shear failure mode under seismic loading. In pre-processing stage, geometry and boundary conditions, element types, material properties and nonlinear analysis solution are defined. Finite element simulation of the complex behavior of concrete as a non-homogeneous and anisotropic material is a challenge in the finite element analysis of reinforced concrete structures and their components. Among constitutive models defining concrete nonlinear behavior as a quasi-brittle material available in ABAQUS, such as smeared and brittle cracking models, the Concrete Damage Plasticity (CDP) is selected and introduced to the numerical model. The main and essential elements of any model based on classical plasticity theory, which are the "yield criteria", "flow rule" and "hardening rule" are all effectively considered in damage plasticity model. Numerical modeling of RC joint shear behavior calibrated by experimental results of other researchers is the main strategy of this study. To verify the model, two RC beam-column connections with exterior and interior joint configurations are selected and simulated. The numerical modeling is first calibrated by experimental results of a quasi-static cyclic test on a half scale exterior beam-column connection which is previously done by Clyde et al (2000) and then applied to an interior full scale RC beam-column connection which is tested by Hakuto et al (2000) under simulated cyclic load. In both cases the ultimate failure of specimens were attributed to the joint shear failure.

2.1 Elements

3D 8-noded hexahedral (brick) elements having 3 degrees of freedom in each node (translations in X, Y and Z directions) are utilized for modeling concrete elements with reduced integration (C3D8R) to prevent the shear locking effect. In order to model reinforcements, 2-noded truss elements (T3D2) having 3 degrees of freedom in each node (translations in X, Y and Z directions of global coordinates system) are used. The embedded method with perfect bond between reinforcement and surrounding concrete is adopted to properly simulate the reinforcement-concrete bonding interaction. It is notable that the effects usually associated with reinforcement-concrete interface, such as bond slip and dowel action are modeled indirectly by defining "tension stiffening" into the reinforced concrete model to approximately simulate load transfer across cracks through the rebar (ABAQUS user's manual (2014)).

2.2 Analysis Approach

Finite Element Analysis (FEA) of the connection joint specimens is performed in a nonlinear static analysis format and the analysis procedure considers both material and geometric nonlinearities. In a nonlinear analysis, the total specified loads acting on a finite element body will be divided into a number of load increments. At the end of each increment the structure is in approximate equilibrium and the stiffness matrix of structure will be modified in order to reflect nonlinear changes in structure's stiffness.

ABAQUS/Standard uses the Newton-Raphson method to obtain solutions for nonlinear problems. Newton–Raphson equilibrium iterations provide convergence at the end of each load increment within tolerance limits for all degrees of freedom in the model. Residual load vector, which is the difference between the internal forces (the loads corresponding to the element stresses) and the external applied loads are analyzed again by Newton–Raphson approach. Subsequently, the program carries out a linear solution using residual loads and considering initial stiffness of structure, in order to check the convergence criteria. If the residual load vector is less than the current tolerance value, the external and internal forces are in equilibrium (this tolerance value is set to 0.5% of an average force in the structure, averaged over time). If convergence criteria are not satisfied, the stiffness matrix is updated, the residual load vector is re-calculated and a new solution is achieved. ABAQUS/Standard also checks that the displacement correction is small relative to the total incremental displacement and it is regularized in such a way that both convergence checks (loads and displacements) must be satisfied before a solution considered to be converged for that load increment.

2.3 Concrete Damage Plasticity Model

Concrete damage plasticity is used as the governing concrete material plasticity model over the whole geometry of the specimens. The model is a plasticity-based model which is developed using concepts of continuum damage mechanics and the application of scalar damaged elasticity in combination with isotropic tensile and compressive plasticity to properly represent the inelastic behavior of concrete (Lubliner et al. (1989)). The main two failure mechanisms of the concrete material are tensile cracking and compressive crushing according to fundamental assumptions of damage plasticity model. The evolution of the yield (or failure) surface and the degradation of elastic stiffness in damage plasticity model are controlled by two hardening variables which are tensile and compressive equivalent plastic strains ($\tilde{\varepsilon}_t^{\,pl}$ and $\tilde{\varepsilon}_c^{\,pl}$). Increasing values of the hardening variables leads to the initiation of micro-cracking and progressive propagation of cracks or the occurrence of crushing in the concrete material. The mentioned yield surface was then modified by Lee and Fenves (1998) in order to take into account the different evolution of concrete tensile and compressive strengths. The current yield surface is defined in the form of effective stresses according to Eq. (1):

$$F\left(\bar{\sigma},\tilde{\varepsilon}^{pl}\right)=\frac{1}{1-\alpha}\left(\bar{q}-3\alpha\bar{p}+\beta\tilde{\varepsilon}^{pl}\left\langle\hat{\bar{\sigma}}_{\max}\right\rangle-\gamma\left\langle-\hat{\bar{\sigma}}_{\max}\right\rangle\right)-\bar{\sigma}_c\left(\tilde{\varepsilon}_c^{pl}\right) \tag{1}$$

Where $\langle x\rangle=\frac{(|x|+x)}{2}$ denotes the Macaulay bracket function. In Eq. 1, $\bar{p}$ is the effective hydrostatic pressure stress and $\bar{q}$ is the Mises equivalent effective stress. These two parameters are stress invariants of the effective stress tensor which are used by the yield surface and plastic flow potential function (Lubliner et al (1989)). $\hat{\bar{\sigma}}_{\max}$ is the algebraically maximum eigenvalue of the deviatory part of effective stress tensor ($\bar{\sigma}$).The parameters α, β and γ in Eq. 1 are dimensionless material constants. Further details on how these parameters affect the damage plasticity model have been dis-

cussed by Lubliner et al (1989) and a summary of their definitions is presented in subsequent paragraphs. The function β is defined as:

$$\beta\left(\tilde{\varepsilon}^{pl}\right)=\frac{\bar{\sigma}_c\left(\tilde{\varepsilon}_c^{pl}\right)}{\bar{\sigma}_t\left(\tilde{\varepsilon}_t^{pl}\right)}(1-\alpha)-(1+\alpha) \tag{2}$$

Here $\bar{\sigma}_c\left(\tilde{\varepsilon}_c^{pl}\right)$ and $\bar{\sigma}_t\left(\tilde{\varepsilon}_t^{pl}\right)$ are effective compressive and tensile cohesion stresses, respectively. In biaxial compression with the maximum principal effective stress equal to zero ($\hat{\bar{\sigma}}_{\max}=0$), the yield surface function of Eq.1 reduces to Drucker-Prager yield condition in which the only parameter needed to define the yield surface is α. The parameter α then can be obtained by comparing the initial equibiaxial and uniaxial compressive yield stresses σ_{b0} and σ_{c0} according to Eq.3:

$$\alpha=\frac{\left(\sigma_{b0}/\sigma_{c0}\right)-1}{2\left(\sigma_{b0}/\sigma_{c0}\right)-1} \tag{3}$$

Typical values of the ratio $(\sigma_{b0}/\sigma_{c0})$ for concrete based on experimental results are reported in the range from 1.10 to 1.16, yielding values of α between 0.08 and 0.12 (Lubliner et al (1989)). Finally, the parameter γ determines the shape of the yield surface in the plasticity model and enters the yield function only for stress states of triaxial compression, when $\hat{\bar{\sigma}}_{max}<0$. The γ coefficient can be determined by comparing the yield conditions along the tensile and compressive meridians. This coefficient is obtained according to Eq.4:

$$\gamma=\frac{3(1-K_c)}{2K_c-1} \tag{4}$$

The coefficient K_c is the ratio of the hydrostatic effective stress in tensile meridian to that on the compressive meridian when the maximum principal stress is negative**.** This coefficient defines the shape of yield surface in the deviatory plane. The shape of deviatory plane was first assumed to be circular as in the classic Drucker-Prager strength hypothesis ($K_c=1$). The CDP model suggests to assume default value of $K_c=2/3$ based on triaxial stress test results. Figure 1 shows a plane stress cross section of the yield surface in principal stress space together with the yield surface cross section on the deviatory plane corresponding to two values of K_c representing different strength criteria.

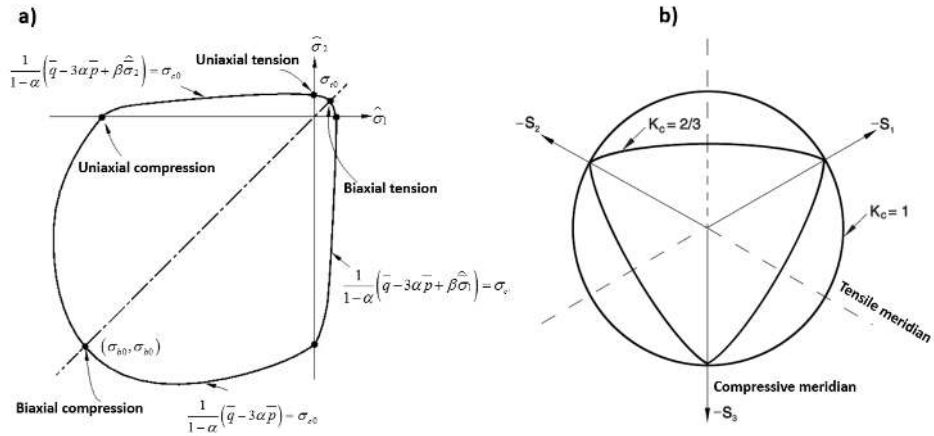

Figure 1: The yield surface in: a) plane stress cross section; b) deviatory plane (Lubliner et al (1989)).

The flow rule in concrete damage plasticity is introduced to the model as an essential element of plasticity theory utilizing non-associated flow potential function $G(\sigma)$. The CDP model uses Drucker-Prager hyperbolic function as non-associated flow potential function according to Eq.5.

$$G(\sigma)=\sqrt{(\in\sigma_{t0}\tan\psi)^2+\bar{q}^2}-\bar{p}\tan\psi \tag{5}$$

The equation involves three material parameters. The first one is dilation angle ψ which is a concrete performance characterizing parameter when it is subjected to triaxial compound stress state. The next parameter $\in$ is eccentricity which adjusts the shape of hyperbola in the plastic potential flow function. The eccentricity parameter is a small positive value and can be estimated as the ratio of concrete tensile strength to its compressive strength. The default value of eccentricity parameter is considered to be equal to 0.1. Finally, the last parameter of plastic flow potential function is the concrete initial uniaxial tensile strength σ_{t0}.

Damage in CDP model is associated with the failure mechanisms consist of concrete cracking and crushing, therefore the occurrence of damage leads to reduction in elastic stiffness. To introduce damage to the model Eq.6 is applied.

$$\sigma=(1-d)\bar{\sigma}=(1-d)E_0:\left(\varepsilon-\varepsilon^{pl}\right) \tag{6}$$

Where E_0 is the initial (undamaged) elastic stiffness of the material and the operator (:) denotes the product of the related tensors. Based on the scalar-damage theory, the stiffness degradation is isotropic and defined by a degradation variable d. Damage is defined in both tensile and compressive states d_t and d_c as functions of plastic strains. Damage parameter can take values in the range from zero (corresponding to undamaged material) to one (corresponding to fully damaged material).

Visco-plastic regularization of the concrete constitutive equations is defined in the numerical model using a generalization of Duvaut-Lions regularization. As a result, the plastic strain tensor

and consequently the stiffness degradation variable were modified. Visco-plastic strain rate tensor ($\dot{\varepsilon}_{\upsilon}^{pl}$) is defined according to Eq.7:

$$\dot{\varepsilon}_{\upsilon}^{pl} = \frac{1}{\mu}\left(\varepsilon^{pl} - \varepsilon_{\upsilon}^{pl}\right) \tag{7}$$

Here ε^{pl} is the evaluated plastic strain and the visco-plastic stiffness degradation variable d_{υ} is defined according to Eq.8:

$$\dot{d}_{\upsilon} = \frac{1}{\mu}\left(d - d_{\upsilon}\right) \tag{8}$$

Where d is the evaluated degradation variable. The stress-strain relation based on viscoplastic model is defined according to Eq.9:

$$\sigma = \left(1 - d_{\upsilon}\right) E_0 : \left(\varepsilon - \varepsilon_{\upsilon}^{pl}\right) \tag{9}$$

2.4 Material Model

2.4.1 Concrete Material Modeling

Uniaxial stress-strain behavior of concrete is simulated utilizing Hognestad type parabola (Hognestad (1951)). The uniaxial stress-strain behavior of concrete can be categorized into three main domains. The first one represents the linear-elastic branch which continues to reach the stress level of σ_{co} that is taken as $\sigma_{co} = 0.4 f_c'$. The second stage shows the hardening part of the concrete uniaxial compressive stress-strain behavior which describes the ascending branch of the stress–strain relationship reaching to the peak load at the corresponding strain level $\varepsilon_0 = 2 f_c'/E_c$. The last part of concrete uniaxial compressive stress-strain relationship attributes to the post-peak softening behavior and therefore represents the initiation and progression of compressive damage in the concrete material until the ultimate compressive strain ε_u. Figure 2 shows the compressive stress-strain behavior of concrete which is introduced to the presented numerical model.

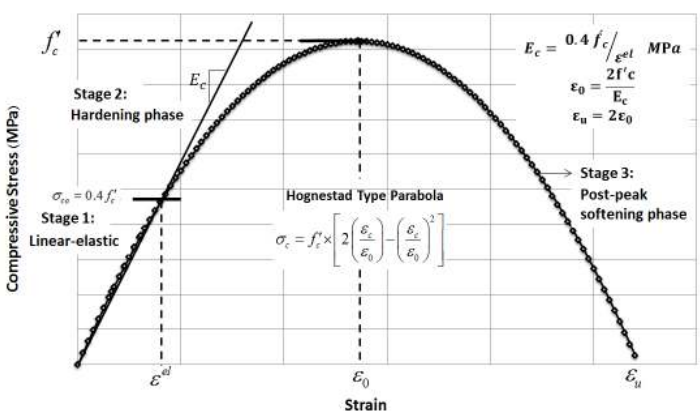

Figure 2: Concrete uniaxial compressive stress-strain diagram.

The uniaxial stress-strain behavior of concrete in tension consists of two parts. As shown in Figure 3, the first part is a linear elastic behavior up to concrete tensile strength σ_{t0}. The second phase initiates together with crack occurrence and its propagation in concrete material under tension demonstrating a descending branch in the uniaxial tensile stress-strain diagram. The behavior in this phase is modeled by a softening procedure which can be modeled using linear, bilinear or nonlinear stress-strain relationships (Belarbi and Thomas (1994)). According to analysis assumptions in this study the linear behavior is applied to the model. Figure 3 demonstrates details of tensile softening assumptions in the presented model.

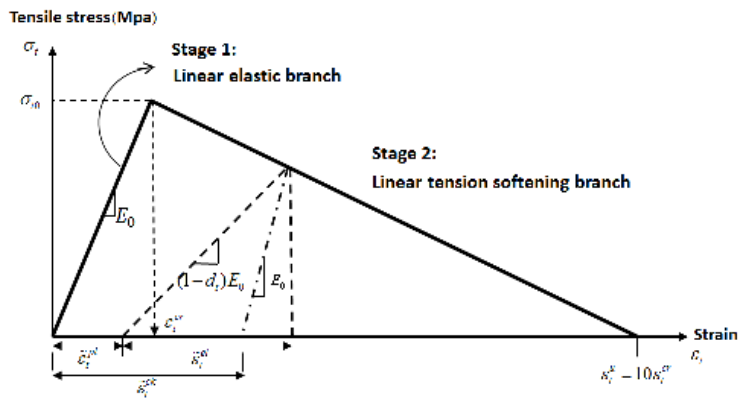

Figure 3: Concrete uniaxial tensile stress-strain behavior and its softening branch assumptions.

The ultimate tensile strength of concrete is estimated by Eq.10 (Genikomsou and Polak (2015) and Wang and Vecchio (2006)).

$$f_t' = 0.33\sqrt{f_c'} \quad \text{(MPa)} \tag{10}$$

Damage is defined both for uniaxial tension and compression during softening procedure in concrete damage plasticity model. Damage in compression occurs just after reaching to the maximum uniaxial compressive strength corresponding to strain level ε_0. The degradation of elastic stiffness in softening regime is characterized by two damage variables, d_t and d_c corresponding to tensile and compressive damage, respectively, which are assumed to be functions of the plastic strains. Tensile and compressive damage in concrete damage plasticity model in the presented numerical model is assumed to be according to equations and diagrams of Figure 4.

2.4.2 Steel Reinforcement Modeling

The uniaxial tensile stress–strain behavior of reinforcement was assumed to be elastic with conventional Young's modulus and Poisson's ratio. The plastic behavior is also modeled including yield stress and corresponding plastic strain. Properties of plastic phase is defined to the model using bilinear behavior.

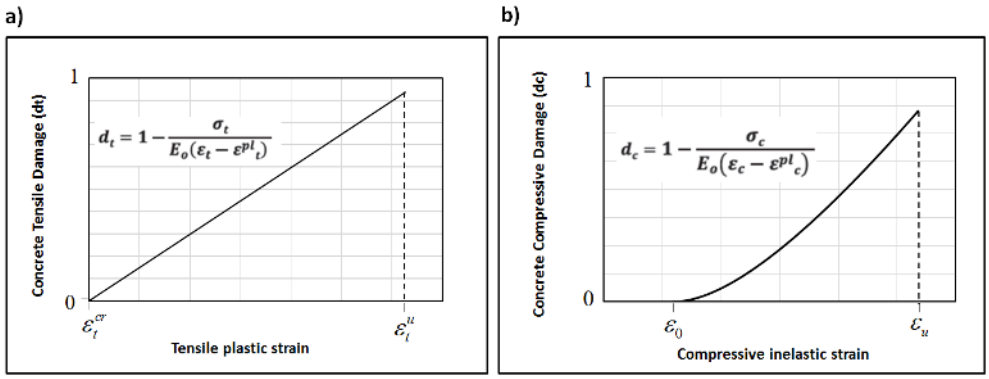

Figure 4: Definition of damage parameter in CDP model:
a) Uniaxial tensile damage; b) Uniaxial compressive damage.

Most finite element studies of RC structures do not consider bond-slip of reinforcing steel and the inherent interaction between reinforcement and concrete in RC members. The post-failure behavior for direct straining is modeled with tension stiffening in CDP model, which helps to define the strain-softening behavior for cracked concrete, therefore in order to consider concrete-reinforcement interaction such as bond slip, an indirect approach which defines "tension stiffening" into the reinforced concrete finite element model is applied as mentioned before in this study. Two different approaches to introduce tension stiffening to the numerical model are the application of post-failure stress-strain relation and the definition and application of fracture energy cracking criterion. The presented numerical model utilizes the first method (post-failure stress-strain relation) to appropriately introduce the tension stiffening behavior of reinforced concrete, the method in which post-failure properties of reinforced concrete is defined by giving the post-failure stress as a function of cracking strain ($\tilde{\varepsilon}_t^{ck}$). Cracking strain is defined as the total strain minus the elastic strain corresponding to the undamaged material according to Eq.11 (Lubliner et al. (1989))

$$\tilde{\varepsilon}_t^{ck} = \varepsilon_t - \varepsilon_{ot}^{el} \tag{11}$$

The elastic strain of undamaged material (ε_{ot}^{el}) is defined according to Eq.12:

$$\varepsilon_{ot}^{el} = \sigma_t / E_0 \tag{12}$$

When unloading data are available the tension softening data can be provided in terms of tensile damage-cracking strain relationship. A linear tension stiffening data based on uniaxial tensile damage definition in CDP model is introduced to the numerical model of the beam-column connections according to the diagram of Figure 5.

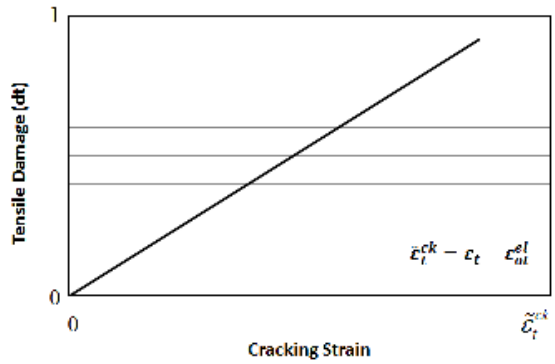

Figure 5: Tension stiffening data introduced to the numerical model in terms of tensile damage-cracking strain linear relationship.

3 VERIFICATION OF THE FINITE ELEMENT MODELING

An exterior half-scale beam-column connection namely test#2 conducted by Clyde et al (2000) and a full scale interior beam-column connection namely unit-01 tested by Hakuto et al (2000) are chosen to validate the numerical model. Both specimens were designed to have joint shear failure as their governing failure mode. To enforce shear failure in the joint, the beam longitudinal reinforcement of exterior beam-column connection was increased to prevent yielding and early degradation of the beam. To represent non-ductile detail of the joint, no transverse reinforcement was considered within the joint panel in both cases (exterior and interior beam-column connections). It is worth mentioning that the interior beam-column connection tested by Hakuto et al (2000) is identical to an interior beam- column connection of an existing RC building constructed in New Zealand before mid-1960s.

3.1 Boundary Conditions, Loading, Dimensions and Details

Geometry and reinforcement details of the exterior and interior joints are shown in Figure 6. A schematic representation of the loading apparatus regarding both test connections is shown in Figure 7. According to boundary conditions applied to the exterior beam-column connection specimen, column was simply supported at both ends and the compressive axial load was applied to the column's end using a hydraulic cylinder. The column axial compressive load is applied to the top of column corresponding to 10% of the compressive strength of concrete in the first step. The lateral load was applied in second step to the beam tip through a loading collar in a quasi-static cyclic manner. The interior beam-column connection had a different boundary condition and loading procedure. The pinned connection at the bottom of the column restrained its lateral displacement, but the column was allowed to rotate and elongate. The ends of the beams were connected by pin-ended steel members to the reaction floor, so that the ends of the beams were free to rotate and to translate horizontally but restrained vertically. No axial load was applied to the column during the test since according to Hakuto et al (2000) the column axial pressure may contribute to the load bearing capacity of the joint making an unfavorable condition. Loading was applied to the interior beam-

column connection in one step only (lateral load). Cyclic horizontal loading was applied to the top end of the columns of the interior test unit using a double acting hydraulic jack.

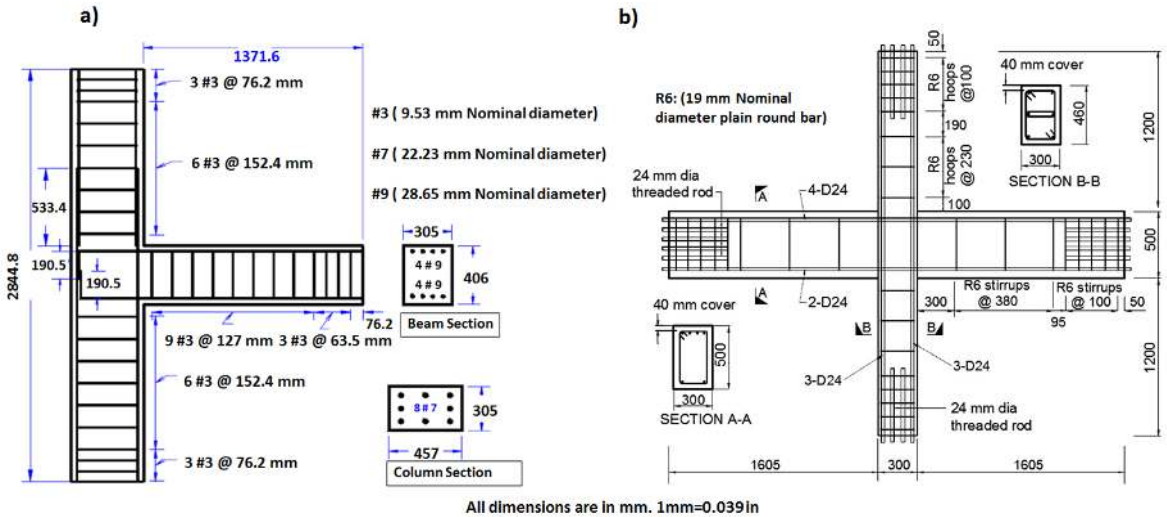

Figure 6: Specimen dimensions and details: a) Exterior beam-column connection (Clyde et al (2000)); b) Interior beam-column connection (Hakuto et al (2000)).

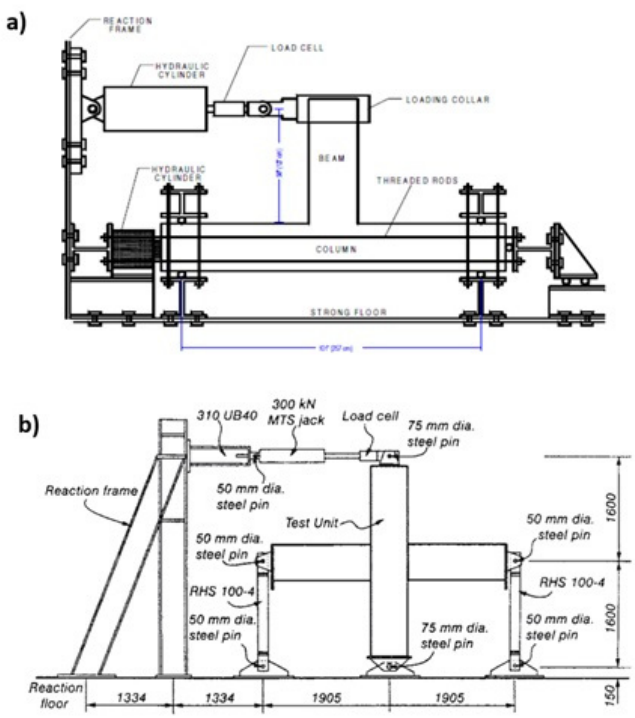

Figure 7: Test setup of beam-column connection specimens: a) Exterior beam-column connection (Clyde et al (2000)); b) Interior beam-column connection (Hakuto et al (2000)).

3.2 Material Properties of the Test Specimens

The measured uniaxial concrete compressive strength of the test specimens, the yield strength and the ultimate tensile strength of reinforcement used in the tests, are reported in Table 1.

Connection specimen	Concrete compressive strength f'_c (MPa)	Reinforcement type	Bar size	Yield strength F_y (MPa)	Ultimate tensile strength F_u (MPa)
Exterior connection (Test #2)	46.2	Beam longitudinal	#9(28.65mm)	454.4	746
		Column longitudinal	#7(22.23mm)	469.5	741.9
		Stirrups	#3(9.53mm)	427.5	654.3
Interior connection (Test 01)	41	Beam and Column longitudinal	D24(24mm)	325	Not reported
		Stirrups	R6(19mm)	339	Not reported

Table 1: Material properties of the test specimens.

4 FINITE ELEMENT ANALYSIS

4.1 Elements

A uniform mesh size of 40 mm is chosen for the concrete elements over the whole geometry in both exterior and interior connection specimens as shown in Figure 8. The same size for reinforcement mesh is also adopted for steel bars. With this configuration, the exterior RC connection specimen has 11144 elements and 13414 nodes and the interior connection has 17414 elements and 21088 nodes. Details regarding element types are presented in Table 2.

Connection specimen	Element type	Element shape	Geometrical order	Number of elements
Exterior connection (Test#2)	C3D8R	Hexahedral	Linear	9536
	T3D2	Line	Linear	1608
Interior connection (Test 01)	C3D8R	Hexahedral	Linear	15328
	T3D2	Line	Linear	2086

Table 2: The number and type of elements in the finite element model.

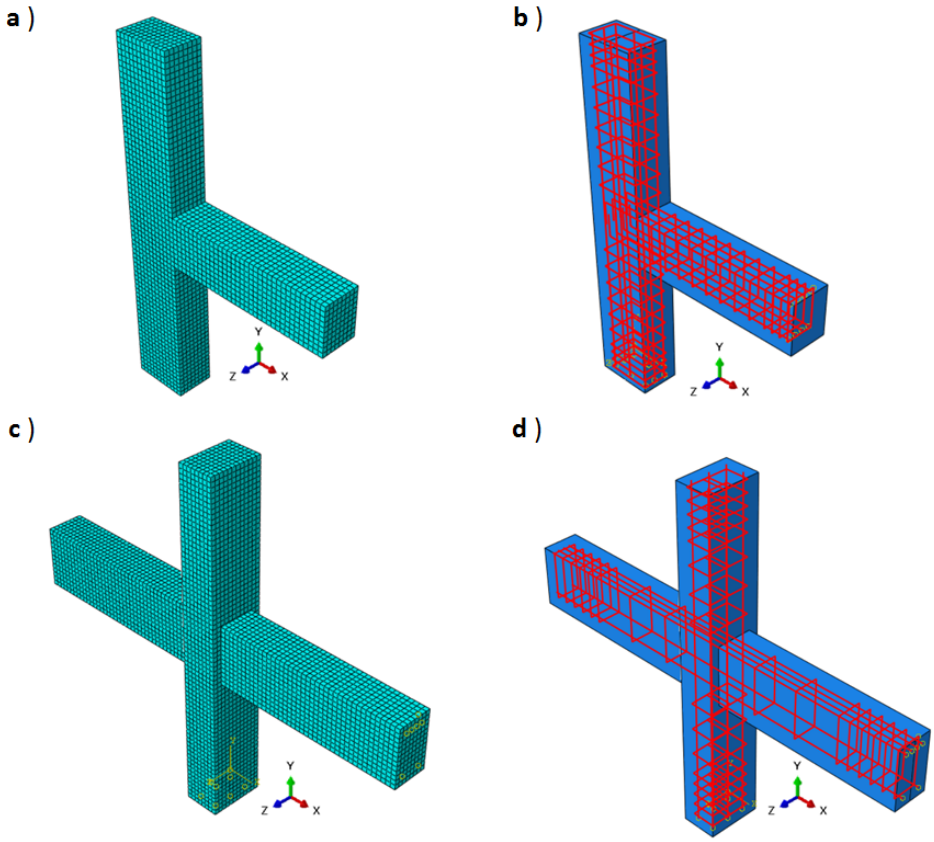

Figure 8: Modeled specimens; a) Concrete element mesh of exterior connection; b) Reinforcement details of exterior connection; c) Concrete element mesh of interior connection and d) Reinforcement details of interior connection.

4.2 Model Geometry and Boundary Conditions

Restraints were defined at both top and bottom surfaces of the specimen's column in the exterior test specimen according to boundary conditions addressed in the test setup. Restraints are also defined in the interior connection specimen according to the test setup boundary conditions both on beam and column tip surfaces. Details regarding to the geometry and boundary conditions of the RC exterior and interior beam-column connections which are applied to the finite element models are illustrated in Figure 9.

Loading is introduced to the model in two separate steps in exterior beam-column connection. The column compressive axial load is applied to the column top surface in the first step which remained constant during the analysis procedure.

The second step corresponds to the monotonic lateral loading of the specimen by applying the lateral displacement at the beam's end surface. However for the interior connection, only one step of load that is related to the lateral loading of the specimen is applied at column's top surface.

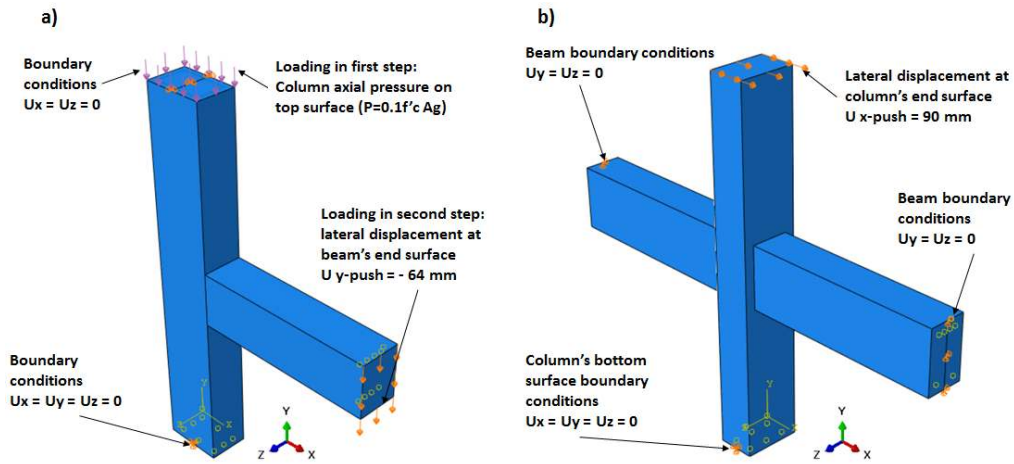

Figure 9: Simulated boundary conditions and loading of the specimens:
a) Exterior beam-column connection; b) Interior beam-column connection.

4.2 Material Parameters and Calibration of the Model

The numerical model is calibrated on the experimental test results of exterior connection specimen as a reference experiment. The calibrated numerical model is then utilized to conduct nonlinear finite element analysis on the interior connection specimen (Test01).

Concrete material parameters used in the presented analysis consists of concrete Young's modulus of elasticity (E_0), Poisson's ratio (ν) and concrete compressive and tensile strengths. The poison's ratio value for concrete material is considered to be equal to 0.2. The concrete damage plasticity input parameters which were discussed in section 2.3 are considered in the plasticity model as presented in Table.3.

Plasticity Parameters	Notation	Parameter's Value considered in the model
Dilation angle	ψ	35° (calibrated)
Shape factor	K_c	0.667 (default value)
Stress ratio	$\frac{\sigma_{b0}}{\sigma_{c0}}$	1.16 (default value)
Eccentricity	ϵ	0.1 (default value)

Table 3: Concrete damage plasticity input parameters.

The uniaxial tensile stress–strain behavior of reinforcement was assumed to be elastic with Young's modulus ($E_s = 2\times10^5 MPa$) and Poisson's ratio ($\nu_s = 0.3$). The plastic behavior is also modeled including yield stress and corresponding plastic strain. Properties of plastic phase is defined to the model using bilinear behavior. Figure 10 illustrates the typical stress-strain relationship of reinforcement introduced to the numerical model. Typical reinforcement properties are also presented in Table 4 for both exterior and interior beam-column connections.

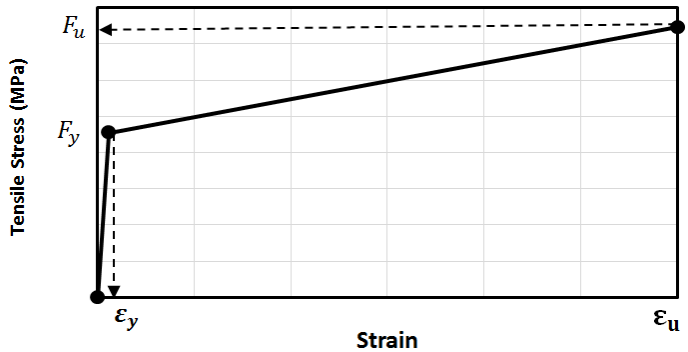

Figure 10: Typical uniaxial stress-strain behavior of reinforcements introduced to the numerical model.

Connection specimen	Reinforcement type	Yield stress $F_y(MPa)$	Yield strain ε_y	Ultimate strength $F_u(MPa)$	Ultimate strain ε_u
Exterior connection (Test#2)	Beam Longitudinal bar	454.4	0.00227	746	0.09
	Column longitudinal bar	469.5	0.00235	741.9	0.09
	Stirrups	427.5	0.00214	654.3	0.11
Interior connection (Test01)	Beam & Column longitudinal bar	325	0.001625	396.5	0.10
	Stirrups	339	0.001695	413.6	0.11

Table 4: Typical stress-strain properties of steel reinforcements.

In order to investigate the role of parameters in constitutive equations of damage plasticity model and to calibrate the model, effects of different logical values of the dilation angle and the viscosity parameter and mesh sensitivity analysis of the model are presented.

The dilatancy of concrete material represents the occurrence of volume expansion when the material is subjected to triaxial stress state and the consequent inelastic strain. Internal actions on the connection joint specimens under simulated lateral loads induce high shear stress in the joint core, an example of which compound stress state leads to considerable dilatancy sensitiveness of the analytical model. A sensitivity analysis on dilation angle as a concrete material parameter is performed to investigate the parameter influence on lateral load-displacement response of the reference specimen. Figure 11 shows that by increasing the value of dilation angle, the displacement capacity and the ultimate failure load of the connection are increased subsequently.

A range between 31° to 42° of the dilation angle parameter is recommended for concrete material according to series of fundamental studies performed by different authors (Lee and Fenves (1988), Wu et al. (2006) and Voyiadjis et al. (2009)). As shown in Figure 11 a value of 35° can reasonably capture the lateral load-deformation curve and the failure mode.

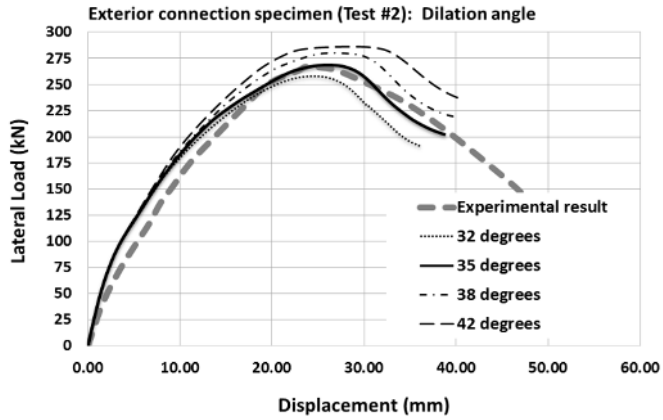

Figure 11: Lateral load-displacement response of FEA for different values of dilation angle.

The influence of visco-plastic regularization on the CDP constitutive equations through the introduction of viscosity parameter was another source of calibration process of the finite element analysis in this study. Defining visco-plastic regularization to the numerical model was first proposed as a method to improve the rate-dependent plastic damage model that brings uniqueness to the incremental stress field in the constitutive equations. It was shown that while the appropriate choice of viscosity parameter and defining it to the model provides relaxation time for visco-plastic system of equations to overcome convergence difficulties in the softening regime, the influence of considering different values of viscosity parameter in monotonic loading cases do not impose considerable amount of changes in the behavior of concrete material under uniaxial tension and compression (Lee (1996)). It was shown that best results are obtained by small values of viscosity parameter compared to the pseudo time of analysis in the study performed by Lee (1996). Series of guidelines and recommendations are suggested by various researchers in order to consider best values of viscosity parameter in the CDP model depending on the type of predominant internal actions which are active and the degree of nonlinearity that involved in different problems (Wosatko et al (2015), Genikomsou and Polak (2015), Wei Ren et al (2015)).

The influence of considering additional relaxation time for the visco-plastic system on the analysis results using different values of viscosity parameter is shown in Figure 12.

According to the diagram of figure 12, the differences in the responses appear only at the softening and to some extent at the hardening regions. For constant element mesh size, when the viscosity parameter was taken as a relative small value of 0.007985, the calculation procedure of the numerical results gave us the most accurate response in comparison to the experimental results. Also the concrete cracking pattern and the nature of joint shear failure were consistent with the test results.

In order to analyze mesh size sensitivity of the numerical model in this study, the finite element analysis results of the exterior connection specimen with 40 mm and 25 mm element mesh sizes are presented in terms of lateral load-displacement curve in Figure 13. Although effects associated with mesh size and strain localization in the presented numerical model are within the margins of error expected for most numerical simulations based on plasticity models, slight differences are observed in the peak lateral loads and displacements.

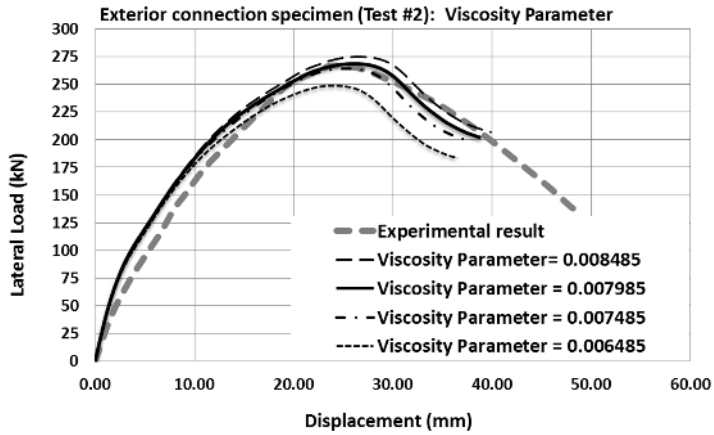

Figure 12: Lateral load-displacement response of FEA for different values of the viscosity parameter.

Slight mesh size dependency is available in most distributed plasticity models which consider strain softening phenomenon in the constitutive equations (Genikomsou and Polak (2015)). It should be investigated that the mesh size dependency does not considerably affect the overall response of the specimen in FEA. It is notable that best results are obtained when the coarse mesh (40 mm) is used which may be due to the fact that most damage processes, causing concrete cracking propagation usually involve length scales in the order of two to three dominant aggregate sizes of the base concrete material (Bazant (1986)).

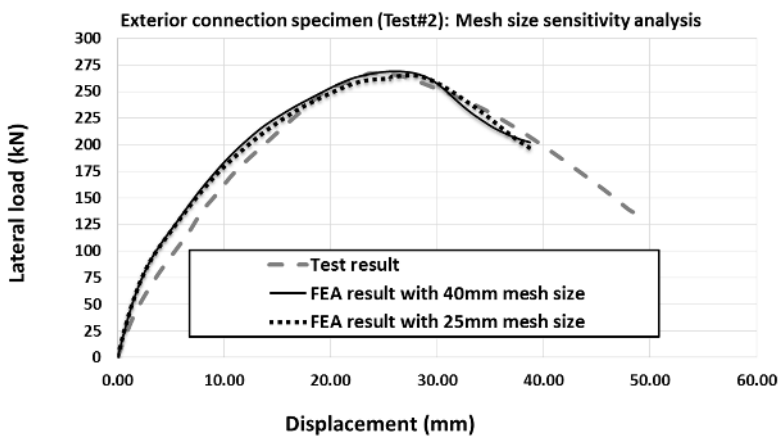

Figure 13: Lateral load-displacement response of RC exterior beam-column connection for 40mm and 25mm mesh sizes.

Among the various methods to reduce the mesh size dependency due to the strain-softening localization in limited number of elements, one method is to introduce the characteristic internal crack length at the softening branch of the stress-strain relationship into the constitutive model. The other method is the introduction of concrete visco-plastic regularization to the numerical mod-

el. The second approach is used in this study but the model is still slightly mesh size dependent however the influence of mesh size dependency on pushover lateral load-displacement behavior of the studied beam-column connections is within the acceptance limits for numerical simulations.

5 FINITE ELEMENT ANALYSIS RESULTS

The FEA results of the RC beam-column connections subjected to lateral loading is presented in terms of force-displacement curves, ultimate loads and displacements and cracking pattern which are monitored at different key points of shear behavior of the connection joints. Comparison between force-displacement curves predicted by simulation and experimental results of exterior and interior connection specimens are presented in Figure 14 and Figure 15, respectively. Figure 14a, and Figure 15a, show the finite element analysis results of force-displacement curves which are compared with the envelope curve of the cyclic loading response shown in Figure 14b and Figure 15b which are obtained by experimental works of Clyde et al(2000) and Hakuto et al(2000) for exterior and interior connection test specimens respectively.

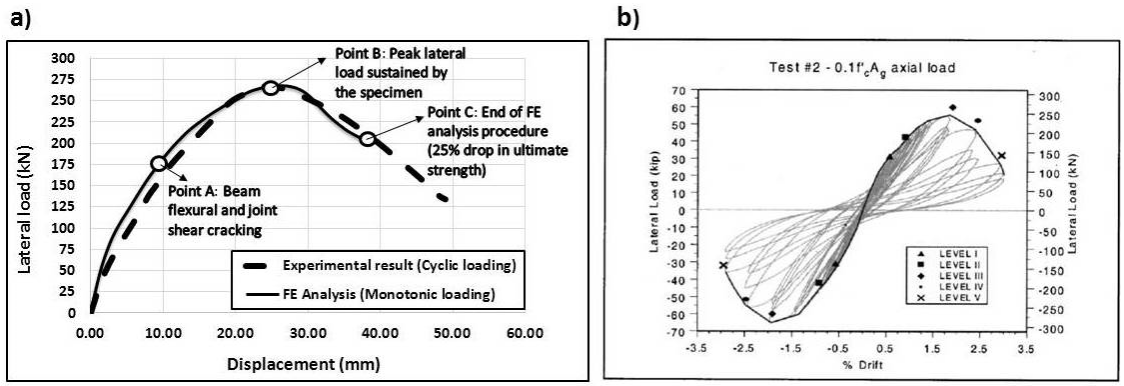

Figure 14: Lateral load-displacement diagrams of exterior Test#2 specimen: a) Comparison between FEA and test; b) Test results of exterior specimen (Test#2) obtained by Clyde et al(2000) experimental study.

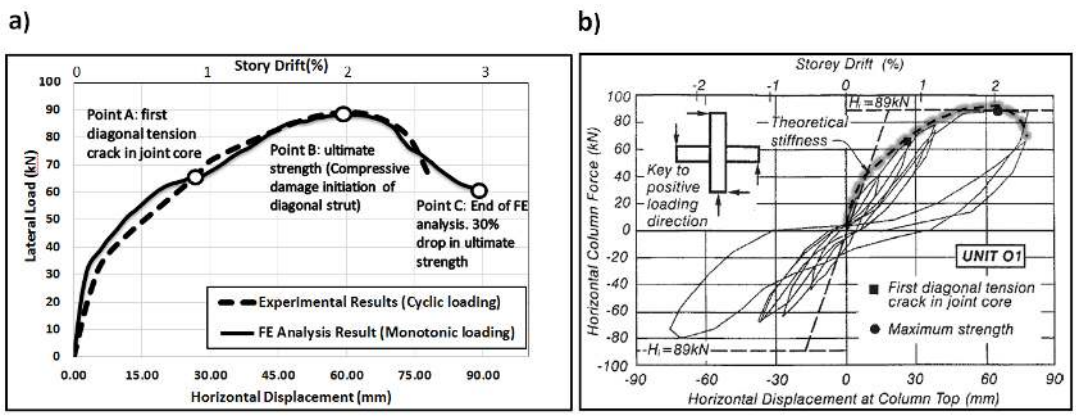

Figure 15: Lateral load-displacement diagrams of interior Test unit 01: a) Comparison between FEA and test; b) Test results of interior specimen (Test unit 01) obtained by Hakuto et al (2000) experimental study.

Peak lateral loads and displacements predicted by the numerical simulation and reported by experimental test results are presented in Table 5.

Connection specimen	Experimental results		Finite element analysis results	
	Peak lateral load (kN)	Displacement at peak lateral load (mm)	Peak lateral load (kN)	Displacement at peak lateral load (mm)
Exterior connection (Test#2)	267	23.77	268.82	24.5
Interior connection (Test 01)	89	60.5	87.38	58.97

Table 5: Ultimate lateral loads and displacements obtained from FEA and experiments.

The finite element analysis shows that the initial response is slightly stiffer than the test results. This may be due to effects of some assumed variables such as the choice of concrete tensile and compressive properties, or the uncertainties often involved with experimental efforts such as probable existence of material deficiencies and also the inherent differences which exist between response obtained by cyclic loading of the experiment and monotonic loading in presented analysis may also contribute in limited stiffer initial response of FEA comparing to testing.

As shown in Figure 14 and Figure 15, three key points of shear behavior that are specified on the FEA resultant lateral load-displacement diagrams for both exterior and interior connection specimens, reasonably match with reported experimental results by Clyde et al (2000) and Hakuto et al (2000), respectively. Point A displays measurable beam flexural and joint shear cracking in exterior specimen and first diagonal shear cracking of the joint core in the interior specimen. Point B displays the ultimate strength of both exterior and interior specimens and finally point C is related to the end of FEA procedure attributed to 25% drop of ultimate strength in exterior connection specimen test and 30% drop of ultimate strength in the interior connection specimen test.

Accuracy of the numerical model in capturing joint shear behavior is monitored through four output parameters which effectively define overall joint shear behavior including concrete tensile and compressive damage, reinforcement output stress and joint cracking pattern. The CDP model simulates the nonlinear behavior of concrete both in tension and compression appropriately. A significant and challenging aspect of damage plasticity model application is the appropriate definition of damage in the constitutive model. The value of maximum principal plastic strain is the main indicator of cracking initiation in concrete damage plasticity model. Cracks initiate when maximum principal plastic strain is positive and the orientation of cracks is considered to be perpendicular to the maximum principal plastic strains, therefore in order to visualize the direction of cracking, the maximum principal plastic strains output is investigated. Figure 16 and Figure 17 display concrete damage both in tension and compression together with reinforcement Von-Mises stress output and joint cracking pattern at three introduced key points of joint shear behavior related to exterior test#2 and interior test unit-01, respectively.

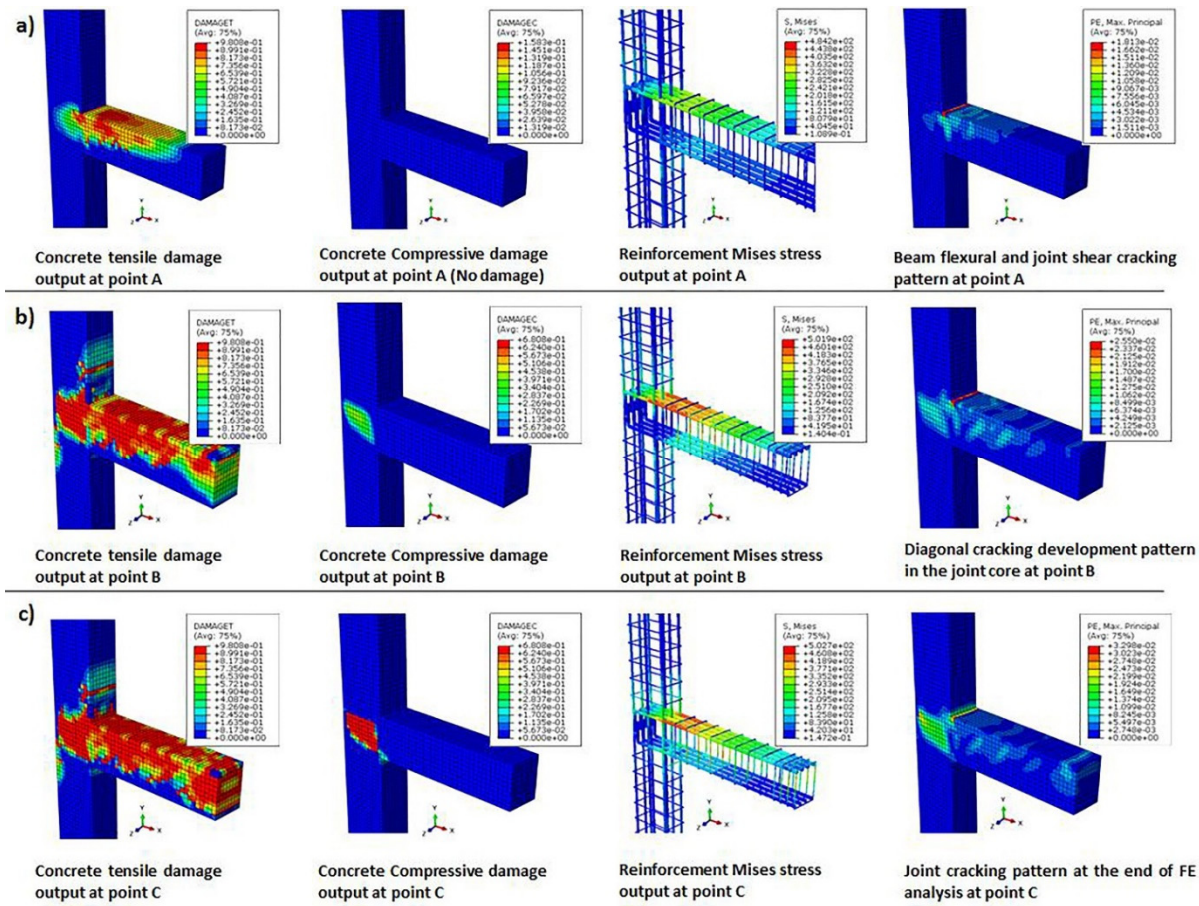

Figure 16: FEA outputs of the exterior beam-column connection specimen at key points of shear behavior: a) Point A; b) Point B; c) Point C.

Exterior beam-column connection specimen experienced beam tensile damage at point A as shown in Figure 16a. The concrete tensile damage extended to the vicinity of the joint and the beam longitudinal bars were placed under tension. No yielding of longitudinal beam bars and also no compressive damage in the joint core were observed at this stage. Measurable flexural cracks in the beam and limited shear cracks in the joint were the main source of slight stiffness change at point A which confirms reported experimental observations at this stage. Limited shear cracking of the joint rapidly spread to the whole joint at point B as shown in Figure 16b. Concrete tensile damage is developed to the joint region followed by yielding of the beam longitudinal reinforcement. The post peak behavior of the connection specimen begins at this point due to compressive damaging of the concrete diagonal strut.

Finally at the end of FEA procedure (point C) corresponding to 25% drop in ultimate strength, the failure of the connection specimen was occurred by crushing of the concrete diagonal strut in the joint region. Figure 16c shows the ultimate joint cracking pattern at point C. The ultimate failure of the beam-column connection specimen is attributed to the joint shear failure as in the experiments. Cracking pattern in the joint region obtained by FEA matches the cracking propagation

pattern observed in the test. The diagonal cracks in the joint region are propagated to vicinity of the column.

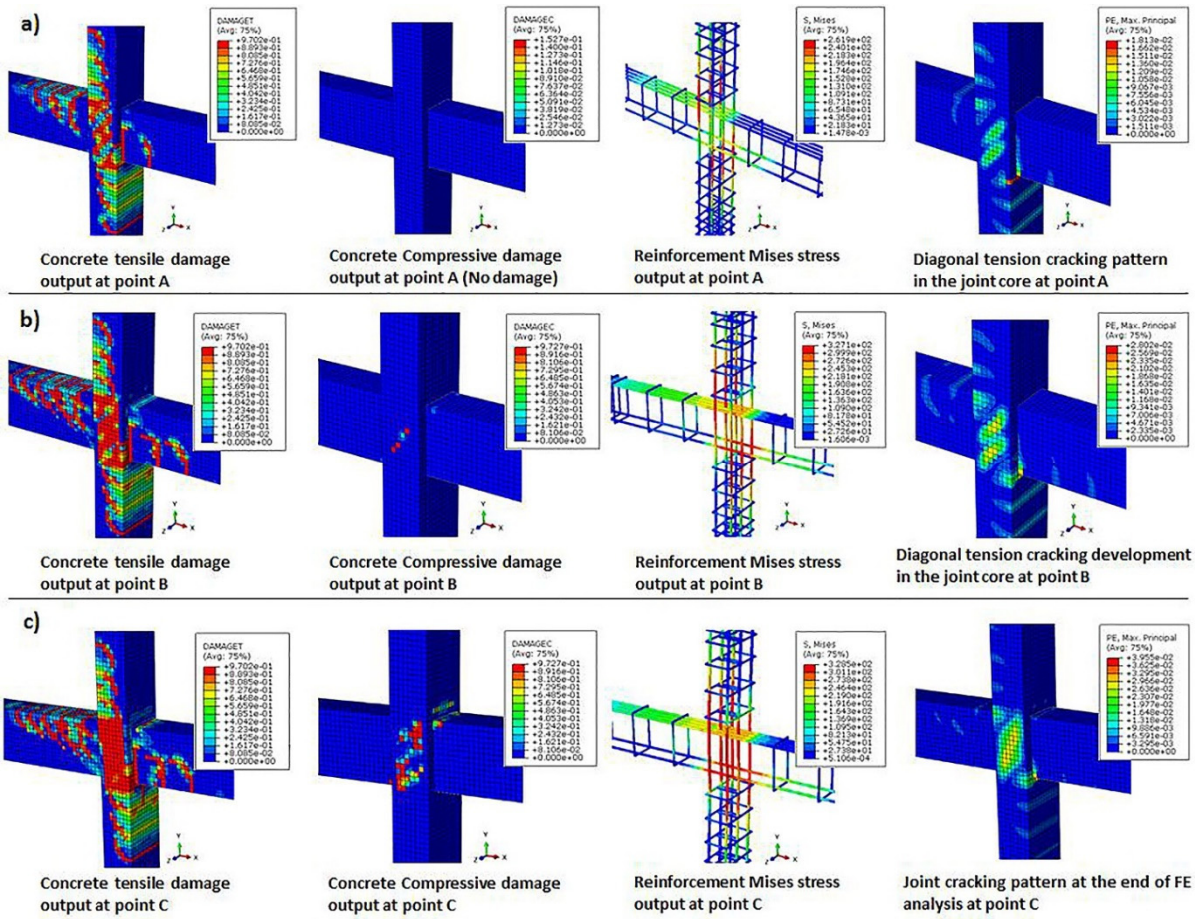

Figure 17: FEA outputs of the interior beam-column connection specimen at key points of shear behavior: a) Point A; b) Point B; c) Point C.

Joint shear behavior described for the exterior beam-column connection specimen is also observed in the numerical output of the finite element analysis performed on the interior beam-column connection. Interior beam-column connection specimen experienced beam tensile damage at beam tension sides together with diagonal concrete tensile damage in the joint core at point A as shown in Figure 17a. Consequently, top of left side beam, bottom of right side beam and longitudinal bars of column on tension side were subjected to tension. No yielding of longitudinal beam bars and also no compressive damage in the joint core were observed similar to the exterior joint numerical output at this stage. Limited flexural cracks in the column and adjacent beams with diagonal tension cracking of the joint core were the main source of stiffness change at point A which is reported in experimental observations and obtained by the FEA outputs. Diagonal tension cracking of the joint rapidly spread to the vicinity of the column at point B as shown in Figure 17b. Concrete tensile damage is developed, and then is followed by yielding of the column and beam longitudinal rein-

forcement in the joint panel zone. The post peak behavior of the connection specimen also begins at this point due to the initiation of compressive damage in the concrete diagonal compressive strut.

Finally at the end of FEA procedure of the interior specimen (point C) corresponding to 30% drop in its ultimate strength, the failure of the connection specimen was occurred by crushing of the concrete diagonal strut in the joint region. As shown in Figure 17c the ultimate failure of the interior beam-column specimen is attributed to the joint shear failure as happened in the experiments. The numerical model shows good agreement between cracking pattern in the joint region obtained by FEA and the cracking propagation pattern observed in the test. Figure 18 presents a comparison between the cracking patterns of the joint region at ultimate strength (point B) for both exterior and interior specimens obtained by the FEA output and observed in the test results.

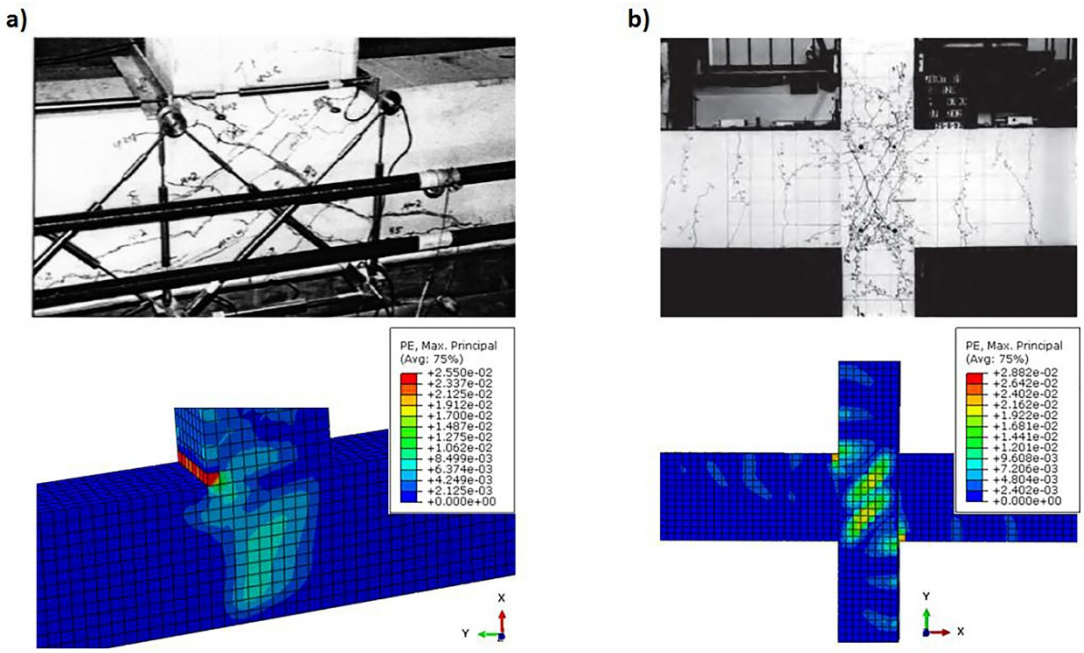

Figure 18: Comparison between joint shear cracking pattern obtained by the FEA output and observed in the test results at point B in: a) Exterior connection specimen; b) Interior connection specimen.

6 CONCLUSIONS

The study presented herein has endeavored to propose a suitable numerical model that describes the nonlinear shear behavior of reinforced concrete beam–column connections including poorly designed and detailed interior and exterior joints. Nonlinear finite element analysis of two RC beam-column connections with exterior and interior configurations is performed in order to capture the joint shear failure as the connection's governing failure mode when subjected to quasi static type lateral load. Concrete damage plasticity material model is applied to the numerical procedure as a distributed plasticity over the whole geometry of the specimens to appropriately simulate material nonlinearity. Two typical beam-column connections in reinforced concrete frame buildings built before the mid-1960s which were tested by other researchers under quasi-static cyclic loading were

chosen as target model for this research. There was no transverse reinforcement considered in the joint panel zone.

The configuration of numerical model is implemented in finite element code ABAQUS. The finite element model is validated with experimental results. Numerical results presented in terms of joint shear capacity, deformations and cracking pattern at introduced key points of joint shear behavior conform appropriately to experimental results. The finite element analysis results confirms the capability of the developed finite element model in this study to predict RC beam-column joint shear behavior and can be further investigated and validated for different types of joints. The model can be used as an efficient and powerful numerical tool for further studies on different RC beam-column joints.

References

ABAQUS Analysis user's manual 6.14-EF (2014). Dassault Systems Simulia Corp. Providence, RI, USA.

ACI 318-14. (2014). Building Code Requirements for Structural Concrete, Reported by American Concrete Institute Committee 318.

ACI 352R-02. (2002). Recommendations for Design of Beam-Column Connections in Monolithic Reinforced Concrete Structures, Reported by Joint ACI-ASCE Committee 352.

ASCE41-13. (2013). Seismic Evaluation and Retrofit of Existing Buildings: American Society of Civil Engineers, Reston, Virginia.

Bazant, Z.P. (1986). Mechanics of distributed cracking, ASME, Applied Mechanics 39(5): P. 227.

Belarbi, A., Thomas, T.C. (1994) Constitutive laws of concrete in tension and reinforcing bars stiffened by concrete. ACI Structural Journal 91(4): 465-474.

Campione, G., Cavaleri, L., Papia, M. (2015). Flexural response of external R.C. beam–column joints externally strengthened with steel cages, Engineering Structures 104: 51–64.

Clyde, C., Pantelides, C.P., Reaveley R.D. (2000). Performance based evaluation of exterior reinforced concrete building joints for seismic excitation. PEER Report 2000/05 Pacific Earthquake Research Center, College of Engineering University of California, Berkeley

Elsouri, A.M., Harajli, M.H. (2013). Seismic response of exterior RC wide beam–narrow column joints: Earthquake-resistant versus as-built joints, Engineering Structures 57: 394-405.

Eslami, A., Ronagh, H. R. (2014) Experimental investigation of an appropriate anchorage system for flange-bonded carbon fiber–reinforced polymers in retrofitted RC beam–column Joints, ASCE J. Composites for Construction 18(4): 04013056.

Esmaeeli E., Barros, J.A.O., Sena-Cruz, J., Fasan, L., Prizzi, F.R.L., Melo, J., Varum, H. (2014). Retrofitting of interior RC beam-column joints using CFRP strengthened SHCC: cast-in-place solution, Composite Structures doi: 10.1016/j.compstruct.2014.12.012.

Esmaeeli, E., Barros, J.A.O., Sena-Cruz, J., Varum, H., Melo, J. (2015). Assessment of the efficiency of prefabricated hybrid composite plates (HCPs) for retrofitting of damaged interior RC beam–column joints, Composite Structures 119: 24–37.

Favvata, M.J., Izzuddin, B.A., Karayannis, C.G. (2008). Modelling exterior beam–column joints for seismic analysis of RC frame structures, Earthquake Engineering and Structural Dynamics 37: 1527–1548.

Genikomsou, A.S., Polak, M.A. (2015). Finite element analysis of punching shear of concrete slabs using damaged plasticity model in ABAQUS, Engineering Structures 98: 38–48.

Guo-Lin Wang, Jian-Guo Dai, Teng, J.G. (2012). Shear strength model for RC beam–column joints under seismic loading, Engineering Structures. 40: 350–360.

Haach, V.G., El Debs, A., El Debs, M. (2008). Evaluation of the influence of the column axial load on the behavior of monotonically loaded RC exterior beam– column joints through numerical simulations. Engineering Structures 30(4): 965–975.

Hakuto, S., Park, R., Tanaka, H. (2000). Seismic load tests on interior and exterior beam- column joints with substandard reinforcing details. ACI structural J. 97(1): 11-25.

Hanson, N.W., Connor, H.W. (1967). Seismic resistance of reinforced concrete beam–column joints. J. Structural Division ASCE 93(5): 533–59.

Hognestad, E. (1951). A study of combined bending and axial load in reinforced concrete members, University of Illinois, engineering experiment station, bulletin series No.399.

Jong-Su Jeon, Shafieezadeh, A., DesRoches, R. (2014). Statistical models for shear strength of RC beam-column joints using machine-learning techniques, Earthquake Engineering and Structural Dynamics. 43: 2075–2095.

Jung-Yoon Lee, Jin-Young Kim, Gi-Jong Oh (2009). Strength deterioration of reinforced concrete beam_column joints subjected to cyclic loading, Engineering Structures 31: 2070_2085.

Kim, J., LaFave, J.M. (2007). Key influence parameters for the joint shear behaviour of reinforced concrete (RC) beam–column connections, Engineering Structures 29: 2523–2539.

Kotsovou G., Mouzakis, H. (2012). Seismic design of RC external beam-column joints. Springer, Bulletin of Earthquake Engineering 10: 645–677.

Kotsovou, G., Mouzakis, H. (2012). Exterior RC beam–column joints: new design approach, Engineering Structures 41: 307–319.

Lee, J., (1996). Theory and implementation of plastic-damage model for concrete structures under Cyclic and Dynamic Loading, Ph.D. Thesis (in English), University of California, Berkeley, USA.

Lee, J., Fenves, G.L. (1998). Plastic-Damage Model for cyclic loading of concrete structures. Journal of Engineering Mechanics. 124(8) (1998) 892-900.

Lima, C., Martinelli, E., Faella, C. (2012). Capacity models for shear strength of exterior joints in RC frames: experimental assessment and recalibration, Springer Bulletin of Earthquake Engineering 10: 985–1007.

Lubliner, J., Oliver, J., Oller, S., Oñate, E. (1989). A plastic-damage model for concrete, International Journal of Solids and Structures 25: 299-329.

Mahini, S.S., Ronagh, H.R. (2011). Web-bonded FRPs for relocation of plastic hinges away from the column face in exterior RC joints, Composite Structures 93(10) (2011) 2460–72.

Maria Teresa De Risi, Paolo Ricci, Gerardo Verderame, M., Gaetano Manfredi. (2016). Experimental assessment of unreinforced exterior beam–column joints with deformed bars, Engineering Structures 112: 215–232.

Masi, A., Santarsiero, G., Lignola, G.P., Verderame, G.M. (2013). Study of the seismic behavior of external RC beam–column joints through experimental tests and numerical simulations, Engineering Structures 52: 207–219.

Mostofinejad, D., Talaeitaba, S.B. (2006). Finite element modeling of RC connections straightened with FRP laminates. Iranian J Science and Technology, Trans B, Eng. 30(B1):21–30.

Muhsen, B.A., Umemura, H. (2011). New Model for Estimation of Shear Strength of Reinforced Concrete Interior Beam-Column Joints, Procedia Engineering 14: 2151–2159.

NEHRP (1997). Guidelines for the seismic rehabilitation of buildings. Federal Emergency Management Agency, FEMA 273

Niroomandi, A., Maheri, A., Maheri, M.R., Mahini, S.S. (2010). Seismic performance of ordinary RC frames retrofitted at joints by FRP sheets, Engineering Structures 32: 2326–2336.

Niroomandi, A., Najafgholipour, M.A., Ronagh, H.R. (2014). Numerical investigation of the affecting parameters on the shear failure of Non-ductile RC exterior joints, Engineering Failure Analysis 46: 62-75.

NZS3101. (2006). Code of practice for the design of concrete structures: Standards Association of New Zealand.

Pantelides, C.P., Hansen, J., Nadauld, J., Reaveley R.D. (2000). Assessment of reinforced concrete building exterior joints with substandard details. PEER Report 2000/05 Pacific Earthquake Research Center, College of Engineering University of California, Berkeley

Park, S., Mosalam, K.M. (2012). Experimental and analytical studies on reinforced concrete buildings with seismically vulnerable beam- column joints. PEER Report 2012/03 Pacific Earthquake Research Center, Department of Civil and Environmental Engineering University of California, Berkeley

Park, S., Mosalam, K.M. (2012). Parameters for shear strength prediction of exterior beam–column joints without transverse reinforcement, Engineering Structures 36: 198–209.

Parvin, A., Granata, P. (2000). Investigation on the effects of fiber composites at concrete joints, Composites Part B Engineering 31(6): 499-509.

Paulay, T., Park, R., Priestley, M.J.N. (1978). Reinforced concrete beam–column joints under seismic actions. ACI J, 75(11): 585–93.

Pauletta, M., Di Luca, D., Russo, G. (2015). Exterior beam column joints shear strength model and design formula, Engineering Structures 94: 70–81.

Saptarshi Sasmal, Ramanjaneyulu, K., Balthasar Novák, Lakshmanan, N. (2013). Analytical and experimental investigations on seismic performance of exterior beam–column subassemblages of existing RC-framed building, Earthquake Engineering and Structural Dynamics 42: 1785–1805.

Sharma, A., Eligehausen, R., Reddy, G.R. (2011). A new model to simulate joint shear behavior of poorly detailed beam–column connections in RC structures under seismic loads, Part I: Exterior joints, Engineering Structures 33: 1034–1051.

Shayanfar, J., Akbarzadeh Bengar, H., Niroomandi, A. (2016). A proposed model for predicting nonlinear behaviour of RC joints under seismic loads, Materials and Design. 95: 563–579.

Shwan, H.S., Abdul Razak, H. (2016). Structural behavior of RC engineered cementitious composite (ECC) exterior beam–column joints under reversed cyclic loading, Construction and Building Materials. 107: 226–234.

Vecchio, C.D., Ludovico, M.D., Prota, A., Manfredi, G. (2016). Modelling beam-column joints and FRP strengthening in the seismic performance assessment of RC existing frames, Composite Structures, doi: http://dx.doi.org/10.1016/j.compstruct.2016.01.077.

Voyiadjis, G.Z., Taqieddin, Z.N. (2009), Elastic plastic and damage model for concrete materials: Part I – Theoretical formulation. Int J Struct Changes Solids – Mech Appl,1(1):31–59.

Wael Kassem. (2016). Strut-and-tie modelling for the analysis and design of RC beam-column joints, Materials and Structures 49(8): 3459–3476.

Wang, P.S., Vecchio, FJ. (2006). VecTor2 and formworks user manual, University of Toronto, Canada.

Wei Ren, Sneed, L.H., Yang Y., Ruili, H. (2015). Numerical simulation of pre-stressed precast concrete bridge deck panels using damage plasticity model, Int J Concrete Struct and Materials, 9(1):45-54

Wong, H.F., Kuang, J.S. (2014). Predicting shear strength of RC interior beam–column joints by modified rotating-angle softened-truss model, Computers and Structures 133: 12–17.

Wosatko, A., Pamin, J., Polak M.A. (2015). Application of damage-plasticity models in finite element analysis of punching shear, Computers and structures 151: 73–85.

Wu, J.Y., Li, J., Faria, R. (2006). An energy release rate-based plastic-damage model for concrete, Int J Solids Struct 43(3):583–612.